

Intensity dependent refractive index in a non-resonant cw Raman laser due to thermal heating of the Raman-active gas

P. A. Roos, J. K. Brasseur*, and J. L. Carlsten

*Montana State University, Department of Physics, Bozeman, MT 59717
roos@physics.montana.edu, Jay.Brasseur@USAF.A.af.mil, carlsten@physics.montana.edu*

* J. K. Brasseur is now with the US Air force Academy, Department of Physics, Laser and Optics Research Center, USAFA, CO 80840

The refractive index of H₂ is shown to decrease linearly as a function of Stokes power and, to a much lesser extent, pump power in a non-resonant cw Raman laser. The dominant source of the index shift is shown to be thermal and significantly larger than dispersion associated with the Raman resonance. A steady state theoretical model based on internal heating due to inelastic Raman scattering events accurately describes the observed behavior. Using this model, frequency pulling of the Raman cavity resonance and phase distortions of the intra-cavity Gaussian beam are predicted for various levels of generated Stokes power.

1. INTRODUCTION

Non-resonant cw Raman lasers have recently been achieved using both frequency-doubled Nd:YAG lasers and diode lasers as pump sources.[1,2] In these systems, stimulation of a Raman transition with such modest cw-range optical power is contingent upon the ability to lock the pump laser frequency to the resonance of a high finesse cavity (HFC) filled with the Raman-active medium. When successfully frequency locked, sufficient optical power can build within the HFC to stimulate the Raman transition even when the pump laser is detuned far from the electronic resonance. However, associated with each of the two non-resonant cw Raman systems achieved were intensity dependent output instabilities observed above the Stokes laser threshold which inhibited frequency locking.[1,2,3] Since the error signal generated for frequency locking was phase sensitive for both systems, the probable cause of the observed instabilities was an intensity dependent refractive index leading to an intensity dependent optical phase shift within the HFC. In this paper, we show that the refractive index of Raman-active molecular hydrogen decreases with increasing Stokes power generated due to heat deposition from the vibrational Raman process.

Numerous studies have been performed on intensity dependent index changes in absorbing gases due to thermal heating [4,5,6,7,8]. However, to the authors' knowledge, no studies of thermal index shifts in Raman-active gases have been conducted. This is most likely because the majority of Raman studies have been performed in the pulsed laser regime where pulse durations are typically much faster than the characteristic time for heat generation, and pulse repetition rates are much slower than characteristic diffusion times. Therefore, under typical circumstances, intensity dependent refractive index effects due to thermal heating in Raman gases are not observable in the pulsed regime. Also, in contrast to the high-Q optical

resonator of cw Raman lasers, absolute phase stability is not a critical parameter for most pulsed systems.

Most previous work in other absorbing gases has concentrated on self-focusing or self-defocusing of a laser beam due to the transverse refractive index gradient across the beam profile. With cw Raman laser systems, of equal concern is the accumulated on-axis phase shift within the HFC regardless of any index gradient since the optical resonator is phase sensitive. The cw Raman laser provides an excellent means to measure such index shifts. The steady-state temporal nature of the output allows accurate measurement of optical effects occurring on time scales slower than typical pulse durations. Also, since the pump power above the Stokes laser threshold remains constant within the laser cavity, the separate index dependencies on pump and Stokes powers can easily be isolated and tested independently. We utilize these advantages to measure the refractive index change in H₂ gas as a function of the pump and Stokes optical powers.

2. THEORY

We model the intensity dependent refractive index by assuming internal heating solely from inelastic vibrational Raman scattering events. This Raman process is illustrated in the energy diagram of figure 1, where a, b, and c represent the ground state, first excited electronic state, and first excited vibrational state respectively, and ν_{pump} , ν_{Stokes} , and ν_{vib} are the frequencies corresponding to the pump laser field, the Stokes laser field, and the first vibrational state respectively. With non-resonant cw Raman lasers, the pump detuning from the electronic resonance, Δ_{pump} , is substantial and the Stokes detuning from the Raman resonance line center, Δ_{Stokes} , can be adjusted by changing the Raman laser resonator length. As can be seen from Fig.

1, associated with the production of each Stokes photon is an energy increase in the Raman gain medium by an amount $h\nu_{vib}$ relative to the ground state. This energy is initially in the form of a molecular vibration, but eventually decays to the ground state, producing heat (shown as a dashed line in Fig. 1). For molecular hydrogen at 12 atm of pressure and room temperature, this decay time is $\sim 30 \mu s$ [9]. Parity conservation forbids radiative transitions directly from state c to a. By measuring the amount of Stokes optical power generated, the amount of heat deposited in the gas can therefore be deduced. The ensuing temperature rise leads to a decrease in refractive index due to a decrease in gas density.

The total power dissipated as heat in the gas between the mirrors of a HFC can be represented in terms of measurable or tabulated parameters by the following equation:

$$P_{heat} = P_{trans} \left(1 + \frac{A_{Stokes}}{T_{Stokes}} \right) \frac{\nu_{vib}}{\nu_{Stokes}} \quad (1)$$

where P_{trans} is the transmitted Stokes power from the HFC, and A_{Stokes} and T_{Stokes} are the HFC mirror power absorption and transmission coefficients respectively at the Stokes wavelength.

Together, P_{trans} and the term in brackets represent the total Stokes optical power generated inside the cavity. The frequency ratio determines the fraction of this optical power that is converted to heat. We assume that the resulting heat power is dissipated into the gas with a Gaussian transverse spatial distribution related to the transverse intensity distribution of the pump beam fundamental HFC mode, giving a power density:

$$Q(r) = B \exp\left(-\frac{2r^2}{\omega_1^2}\right). \quad (2)$$

It should be noted that the confocal parameter for our setup is more than two times the HFC length, so the optical beam waist remains roughly constant throughout the cavity. The $1/e^2$ width of this distribution is given by:

$$\omega_1 = \omega_0 \sqrt{1 + \frac{8D\tau_{vib}}{\omega_0^2}}, \quad (3)$$

where the square root term accounts for broadening of the distribution relative to the optical beam width due to random walk diffusion during the vibrational state decay time τ_{vib} . D is the gas diffusion constant and ω_0 is the minimum beam radius of the optical beam as determined by the mirror spacing and curvature [10]. The normalization constant B is determined by requiring that integration of equation (2) over the HFC volume yield P_{heat} from equation (1). This gives the following relation when the beam waist is much smaller than the HFC inner radial dimension:

$$B \approx \frac{2P_{heat}}{\pi\omega_1^2 L}. \quad (4)$$

Two methods can be used to solve for the resulting steady state temperature distribution inside the HFC. Since the temperature inside the cavity is independent of both the axial and angular dimensions, the diffusion equation can be directly integrated twice with respect to the radial dimension in cylindrical coordinates.[4] Alternatively, a Green's function approach can be used to generate the temperature distribution within the cavity. Following this path, we incorporated the Gaussian power density distribution from equation (2) into equation (10.1.21) of Ref. 11. With a judicious choice of integration by parts, the result obtained is identical to equation (A9) of Ref. 4. Including equation (4) from above, the resulting radial dependence of the steady state temperature within the HFC relative to a constant temperature surface can be described by

$$\Delta T(r, P_{heat}) = \frac{P_{heat}}{4\pi LK} \left\{ 2 \ln\left(\frac{a}{r}\right) + \text{Ei}\left(-\frac{2r^2}{\omega_1^2}\right) - \text{Ei}\left(-\frac{2a^2}{\omega_1^2}\right) \right\}, \quad (5)$$

where r is the radial distance from the beam axis, $Ei(x)$ is the exponential integral function [12], K is the thermal conductivity of the gas, and a is the radius of the constant temperature surface.

The temperature function of equation (5) can be related to refractive index by assuming steady state ideal gas conditions and that the refractivity (n_0-1) is proportional to gas density:

$$\Delta n(r, P_{heat}) = -\frac{(n_0 - 1)}{T_0} \Delta T(r, P_{heat}), \quad (6)$$

where T_0 and n_0 are the temperature and refractive index in the absence of optical power.

Combining equations (1), (5), and (6) yields

$$\Delta n(r, P_{trans}) = \frac{P_{trans}}{4\pi L K} \left(\frac{1 - n_0}{T_0} \right) \left(1 + \frac{A_{Stokes}}{T_{Stokes}} \right) \frac{v_{vib}}{v_{Stokes}} \left\{ 2 \ln \left(\frac{a}{r} \right) + Ei \left(-\frac{2r^2}{\omega_1^2} \right) - Ei \left(-\frac{2a^2}{\omega_1^2} \right) \right\}. \quad (7)$$

This gives the predicted index change as a function of radial distance and transmitted Stokes power. The function cannot be evaluated on the beam axis ($r=0$), but the near-axis value can be approximated in analogy with equation (A14) from Ref. 4 when $r \ll \omega_1 \ll a$ with the following result:

$$\Delta n(r, P_{trans}) \approx \frac{P_{trans}}{4\pi L K} \left(\frac{1 - n_0}{T_0} \right) \left(1 + \frac{A_{Stokes}}{T_{Stokes}} \right) \frac{v_{vib}}{v_{Stokes}} \left[\ln \left(\frac{2\gamma a^2}{\omega_1^2} \right) - \frac{2r^2}{\omega_1^2} \right], \quad (8)$$

where $\gamma \approx 1.78$ is Euler's constant. The accumulated phase shift over the length of the cavity and the HFC resonant frequency shift for the pump beam can be calculated from either of the previous two expressions using the relations

$$\Delta \phi(r, P_{trans}) \approx 2\pi \frac{L}{\lambda_{pump}} \Delta n(r, P_{trans}) \quad (9)$$

and

$$\Delta \nu(r, P_{trans}) \approx \frac{c}{\lambda_{pump}} \Delta n(r, P_{trans}), \quad (10)$$

where c is the speed of light and λ_{pump} is the pump wavelength. The resulting expression for the phase shift is independent of cavity length for a given spot size, but there is an implicit dependence on length in the calculation of ω_1 .

3. EXPERIMENT

The experimental setup for measuring refractive index changes is shown in figure 2. The pump source is a frequency-doubled cw Nd:YAG operating at 532 nm which can be temperature tuned over a range of roughly 10 GHz. Two optical isolators are used to minimize optical feedback resulting in ~60dB attenuation of back-scattered light. The EOM places 12 MHz sidebands on the carrier frequency for locking purposes. A half-wave plate is used to produce a variable attenuator for the pump. The laser's frequency is stabilized to a HFC resonance using the Pound-Drever-Hall method.[13] The HFC consists of two mirrors with curvature of +25 cm, spaced by three piezo-electric transducer (PZT) tubes, giving a cavity length of 7.6 cm. This cavity is placed within a hermetically sealed housing filled with 12 atm of diatomic hydrogen gas. To maintain resonance within the cavity, fast (<200 kHz) frequency corrections are made to the Nd:YAG laser output by double-passing an AOM. Slow (<20 kHz) corrections are performed on the cavity resonance frequency by changing the HFC mirror spacing via the PZT tubes. In this manner, changes in optical path length between the HFC mirrors due to refractive index shifts are manifest as changes in applied PZT voltage as the system adjusts the physical path length between the mirrors in order to maintain resonance within the optical cavity.

During measurement, the Stokes output power and PZT voltage applied by the servo are monitored as functions of input pump optical power both below and above the Stokes laser threshold. In order to minimize the effects of long term PZT and temperature drifts not

associated with the optical power, reference data points are taken between each of the signal data points at a fixed pump level well below threshold. The slow background drifts evident in the reference data can be removed from the signal data leaving only the effects associated with the optical power. Also, data within a single set are taken for both increasing and decreasing pump power values to expose any hysteresis effects. The time between successive measurements is ~ 12 s, while the diffusion time for gas molecules out of the beam is on the order of 1 ms. Therefore, steady state conditions are expected to prevail. To ensure that the PZT movement is not in response to DC frequency shifts generated by the AOM, the laser frequency is monitored with 10 MHz resolution after the AOM as shown in Fig. 2.

4. RESULTS AND DISCUSSION

Figure 3 shows the resulting voltage applied to the PZT as a function of pump optical power coupled into the HFC when the laser frequency is tuned to line center of the ~ 610 MHz Raman resonance. A clearly defined change in behavior is observed beyond ~ 850 μW which corresponds to the Stokes laser threshold. Note that above this threshold, the intra-cavity pump power remains roughly constant.

The measured PZT voltages were converted into corresponding refractive index changes using the following relation:

$$\Delta n = - \left(\frac{\Delta V_{meas}}{\Delta V_{FSR}} \right) \left(\frac{\lambda_{pump}}{2L} \right) \quad (11)$$

where ΔV_{FSR} is the PZT voltage corresponding to one free spectral range (FSR) of the Raman cavity, L is the cavity length, and the negative sign is due to the fact that the cavity length decreases for increasing PZT voltage. Figure 4 shows the resulting index change as a function of

transmitted Stokes power for the cases when the cavity was tuned to line center ($\Delta_{\text{Stokes}}=0$) and to the positive half-width ($\Delta_{\text{Stokes}}=305$ MHz) of the Raman resonance. The solid lines represent linear fits to the measured data for Stokes power greater than zero. From these slopes, the index change with Stokes power is observed to be independent of detuning to within measurement uncertainty. Detuning the cavity to the negative half-width of the Raman resonance yields statistically indistinguishable results from that on the positive frequency side. This indicates that the observed effect is dominated by thermally induced index changes rather than by dispersion associated with the Raman resonance, since for the latter, the sense of the index change for the two detuned data sets would be reversed with respect to one another.

The dashed lines in Fig. 4 represent the predicted on-axis index dependence on transmitted Stokes power from equation (8) with $r=0$ for two values of the constant temperature surface radius, a . The two radii reflect the actual HFC geometry which consists of two coaxial aluminum cylinders with inner radii of 1.2cm and 2.4cm respectively, neither of which are temperature stabilized. The following measured or tabulated parameters were used to generate these curves: $n_0-1=1.564\times 10^{-3}$ [14], $T_0=293$ K, $\omega_l=135\mu\text{m}$, $L=7.6\text{cm}$, $K=2.18$ mW/cm²*K [14], $A_{\text{Stokes}}=108$ ppm, $T_{\text{Stokes}}=122$ ppm, $\nu_{\text{vib}}/c=4155$ cm⁻¹ and $\nu_{\text{Stokes}}/c=14640$ cm⁻¹. The constant temperature radius giving the best agreement with the measured slope falls between the two physical radii actually present in the HFC. Thus, the model provides an accurate description of the index behavior with Stokes power on axis. The offset of the measured data relative to the origin on the vertical axis is addressed below. This model neglects convection in the gas and optical losses in the HFC other than those due to the absorption and transmission of the cavity mirrors. We have assumed heating solely due to inelastic Raman scattering events and that there is no longitudinal heat flow along the axis of the cavity. Also, the on-axis values are used in the

calculation, while in reality, a slight index gradient over the width of the beam exists. This index gradient is predicted to be negligible for the Stokes power levels generated in this study, as shown below.

The predicted index change can also be predicted as a function of radial distance from the beam axis, using equation (7) from above. This dependence is shown in figure 5 for the same two constant temperature radii. This analysis assumes a generated Stokes power (combined power absorbed and transmitted by the HFC mirrors) of 1mW. A radial index gradient is predicted, presenting the possibility of thermal self-defocusing. To further illustrate the predicted self-defocusing, figure 6 shows the steady state optical phase accumulated over the cavity length relative to the on-axis value as predicted by equations (7) and (9). Three levels of generated Stokes optical power are given as functions of radial distance from the beam axis out to the beam waist for a constant temperature radius of $a=1.1$ cm. This analysis does not include beam broadening within the cavity as a result of the predicted index gradient. The theory indicates that steady-state thermal phase distortions may begin to affect mode coupling only for higher power systems, which have not yet been realized. For such systems, the lenses used to mode match into the HFC may be adjusted to maximize coupling efficiency.

Equations (8) and (10), with $r=0$, can be used to predict the effect of the on-axis index change on the HFC resonance. Using the same parameters as above, the predicted steady state frequency shift of the HFC resonance due to heating is ~ 30 MHz per milliwatt of generated Stokes power. Since the HFC linewidth is typically much less than 1 MHz, such heating can significantly pull the cavity out of resonance with the pump laser in the absence of corrective measures even for low power systems. The magnitude of this shift can be mitigated by

increasing the resonator length or by decreasing the constant temperature surface radius, although this will adversely effect the index gradient, thereby enhancing self-defocusing.

A subtler index shift associated only with the pump power is also evident in Fig. 4. The linear fits to the measured data do not include the origin within measurement uncertainty. This characteristic was common to all data taken regardless of location on the Raman resonance and indicates that some index shift occurs before the Stokes laser threshold, due only to the input pump power. The detuned case displays a higher vertical axis intercept. This can be explained by noting that the Stokes laser threshold for the detuned case requires twice the input pump power as that for the line center case due to decreased Raman gain. For input pump powers greater than the Stokes laser threshold value, the intra-cavity pump power remains roughly constant. Figure 6 shows the effective index shift as a function of input pump power below the Stokes laser threshold for two different locations on the Raman resonance. Again, the linear slope of the induced index change does not depend on detuning within measurement uncertainty, indicating a thermal source for the index change. The two lines represent linear fits to the measured data. By reversing the calculation used for the Stokes, we can estimate the fraction of the pump power coupled into the cavity that is contributing to heat generation:

$P_{heat}/P_{pump}=0.024$. Possible mechanisms for this heat generation include inelastic Brillouin and Rayleigh scattering.

5. CONCLUSIONS

Intensity dependent refractive index shifts in Raman-active H₂ were found to be dominated by thermal sources in the cw regime. Under typical pulsed laser conditions, thermal effects should not be observable. A steady state theoretical model based on inelastic Raman

scattering events is shown to predict the observed change in index with Stokes power. This index change leads to pulling of the HFC resonant frequency by ~30 MHz per milliwatt of generated Stokes power for the system used in this study. The effect is therefore a significant consideration for cw Raman laser frequency locking, even for low power systems. However, it has been shown in previous work that the resulting output instabilities can be overcome using electronic feedback measures [3]. Thermal self-defocusing effects are also predicted to be significant for higher power systems in the future. Adjustment of mode matching optics should mitigate the resulting pump beam coupling losses into the HFC.

Acknowledgments:

This work is supported by NSF under grant # 9731602.

References:

1. J. K. Brasseur, K. S. Repasky, and J. L. Carlsten, *Opt. Lett.* **23**, 367 (1998).
2. P. A. Roos, J. K. Brasseur, and J. L. Carlsten, *Opt. Lett.*, to be published (1999).
3. J. K. Brasseur, P. A. Roos, K. S. Repasky, and J. L. Carlsten, *J. Opt. Soc. Am. B*, to be published (1999).
4. J. P. Gordon, R. C. C. Leite, R. S. Moore, S. P. S. Porto, and J. R. Whinnery, *J. Appl. Phys.* **36**, 3 (1965).
5. K. E. Rieckhoff, *Appl. Phys. Lett.* **9**, 87 (1966).
6. R. L. Carman, and P. L. Kelley, *Appl. Phys. Lett.* **12**, 241 (1968).
7. S. A. Akhmanov, D. P. Krindach, A. V. Migulin, A. P. Sukhorukov, and R. V. Khokhlov, *IEEE J. Quantum Electron.* **QE-4**, 568 (1968).
8. F. W. Dabby, R. W. Boyko, C. V. Shank, and J. R. Whinnery, *IEEE J. Quantum Electron.* **QE-5**, 516 (1969).
9. M. M. Audibert, C. Joffrin, and J. Ducuing, *Chem. Phys. Lett.* **1**, 26 (1973).
10. A. Yariv, *Quantum Electronics*, 3rd ed. (Wiley, New York, 1989) 140.
11. P. M. Morse and H. Feshbach, *Methods of Theoretical Physics*, (McGraw Hill, New York, 1953) 1191.
12. W. H. Beyer, *CRC Standard Mathematical Tables and Formulae*, 29th ed. (CRC Press, 1991) 373.
13. R. W. P. Drever, J. L. Hall, F. V. Kowalski, J. Hough, G. M. Ford, A. J. Munley, and H. Ward, *Appl. Phys. B* **31**, 97 (1983).
14. D. E. Gray, *American Institute of Physics Handbook*, 2nd ed. (McGraw Hill, New York, 1963). Adjusted for pressure of 12 atm and temperature of 293 K.

Figure Captions:

Figure 1: Energy level diagram for the vibrational Raman process. Decay from the first vibrational state (c) to the ground state (a), represented by a dashed line, is nonradiative and is the source for internal thermal heating of the Raman gas.

Figure 2: Experimental setup for measuring refractive index changes in H₂. The Pound-Drever-Hall method is used to lock the laser's frequency to a resonance of the high finesse cavity (HFC) filled with H₂ in order to stimulate the Raman transition. Refractive index changes in the gas are deduced by monitoring the voltage applied to the PZT as a function of pump and Stokes optical powers. EOM, electrooptic modulator; AOM, acoustooptic modulator; PBS, polarizing beam splitter; MML, mode matching lenses; $\lambda/2$, half-wave plate; $\lambda/4$, quarter-wave plate.

Figure 3: PZT voltage change as a function of pump optical power coupled into the HFC. Note the behavioral change at the Stokes laser threshold ($\sim 850 \mu\text{W}$).

Figure 4: Refractive index change as a function of Stokes optical power. The solid circles represent Raman line center data ($\Delta_{\text{Stokes}}=0$), while the open circles are for the positive half-width detuned case ($\Delta_{\text{Stokes}}=305 \text{ MHz}$). The two solid lines are linear fits to the measured data while the two dashed lines are theoretical predictions based on equation (8) for two different radii of the constant temperature surface. The slopes of the linear fits do not depend on detuning, indicating that the source of index change is thermal

Figure 5: Predicted refractive index change as a function of radial distance from the beam axis for two constant temperature surface radii. This scale illustrates the effect of thermal heating throughout the Raman laser cavity.

Figure 6: Predicted optical phase shift in the Raman laser resonator relative to the on-axis value as a function of radial distance from the beam axis out to the beam waist for three different levels of generated Stokes power. The predictions indicate that self-defocusing may be a consideration for higher power systems.

Figure 7: Refractive index as a function of input pump power below the Stokes laser threshold. The solid line is a linear fit to the line center data (solid circles) while the dashed line is a linear fit to the half-width detuned data (open circles). These slopes do not depend on detuning, indicating a thermal source for the index change.

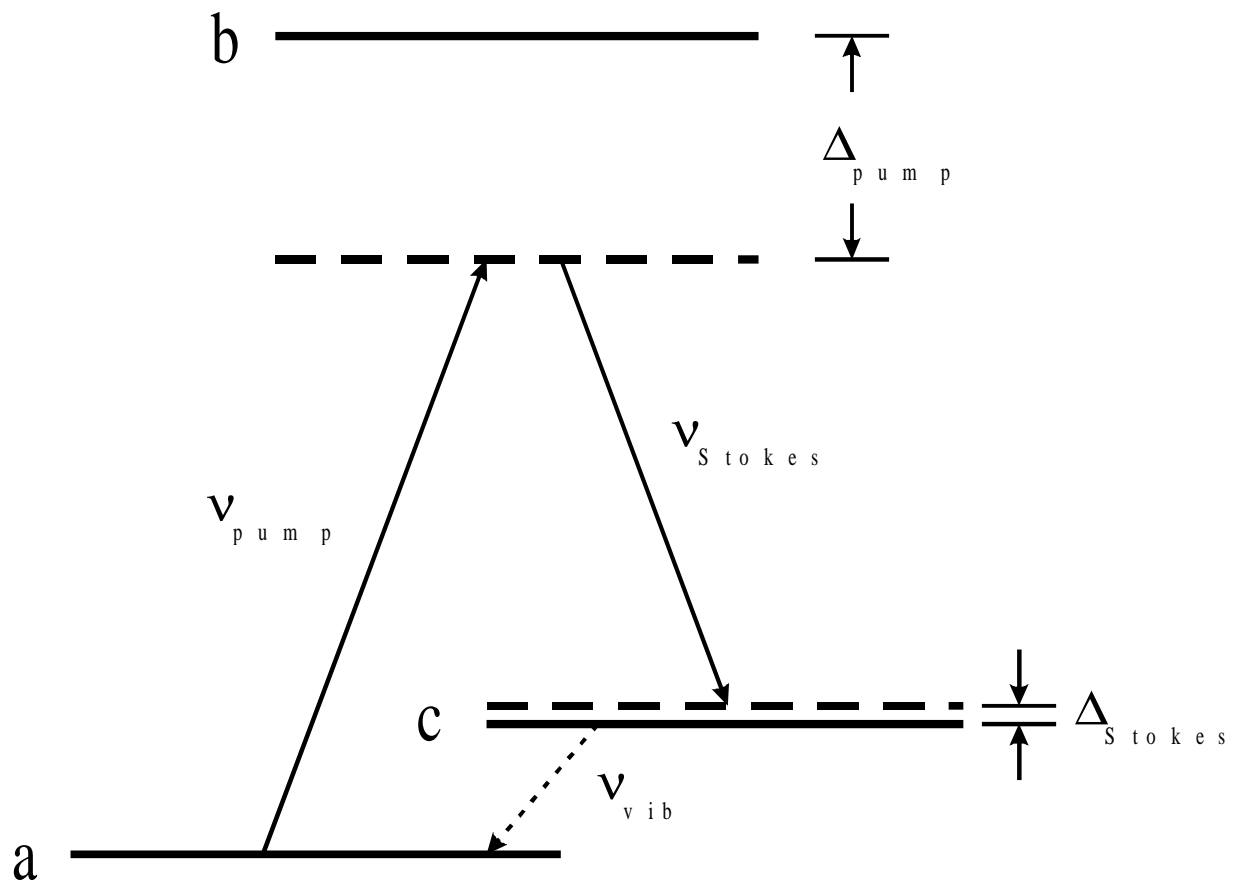


Figure 1

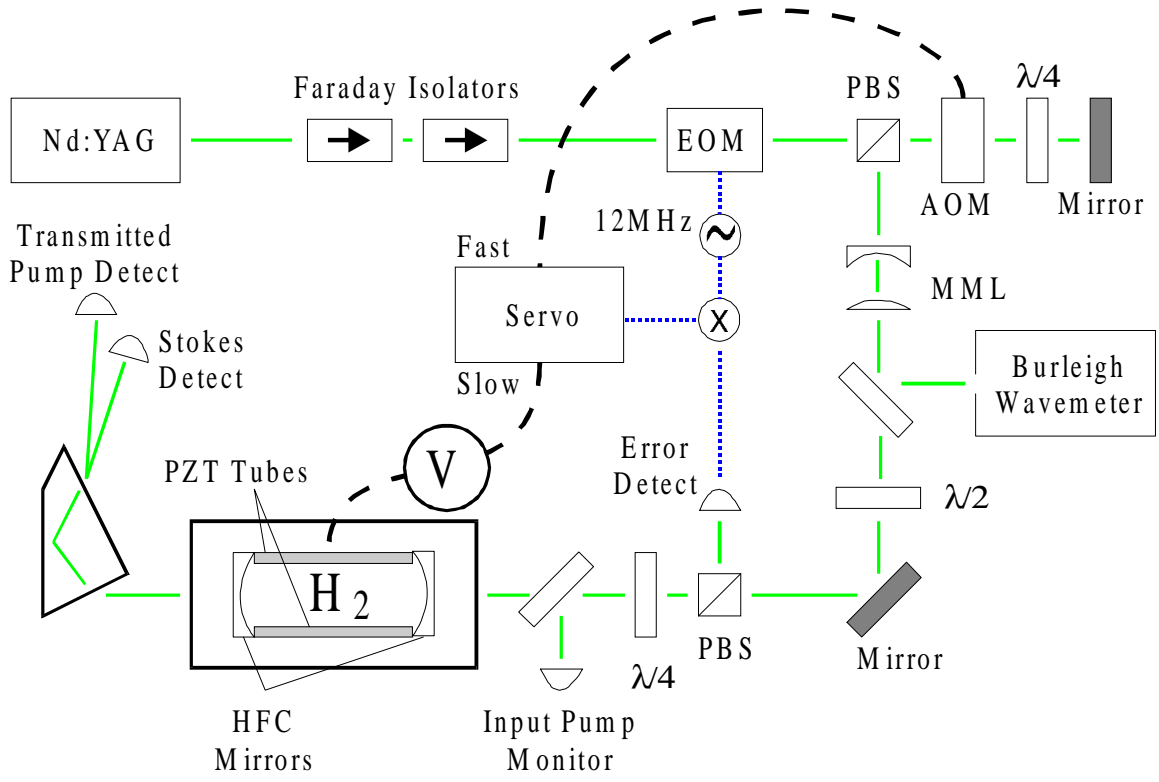


Figure 2

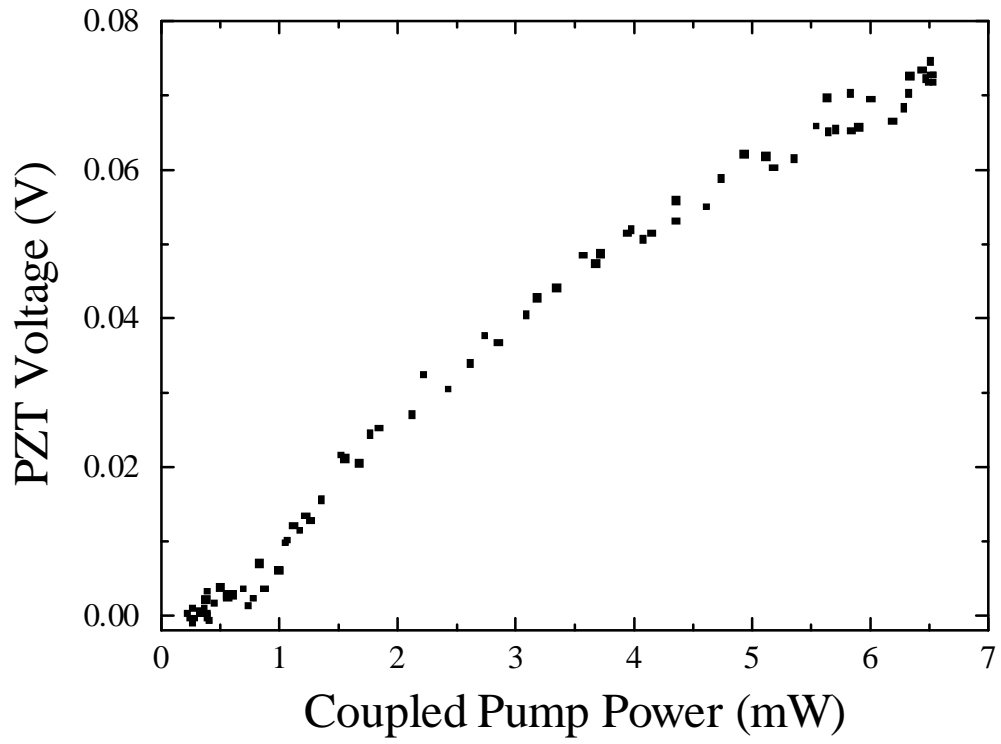


Figure 3

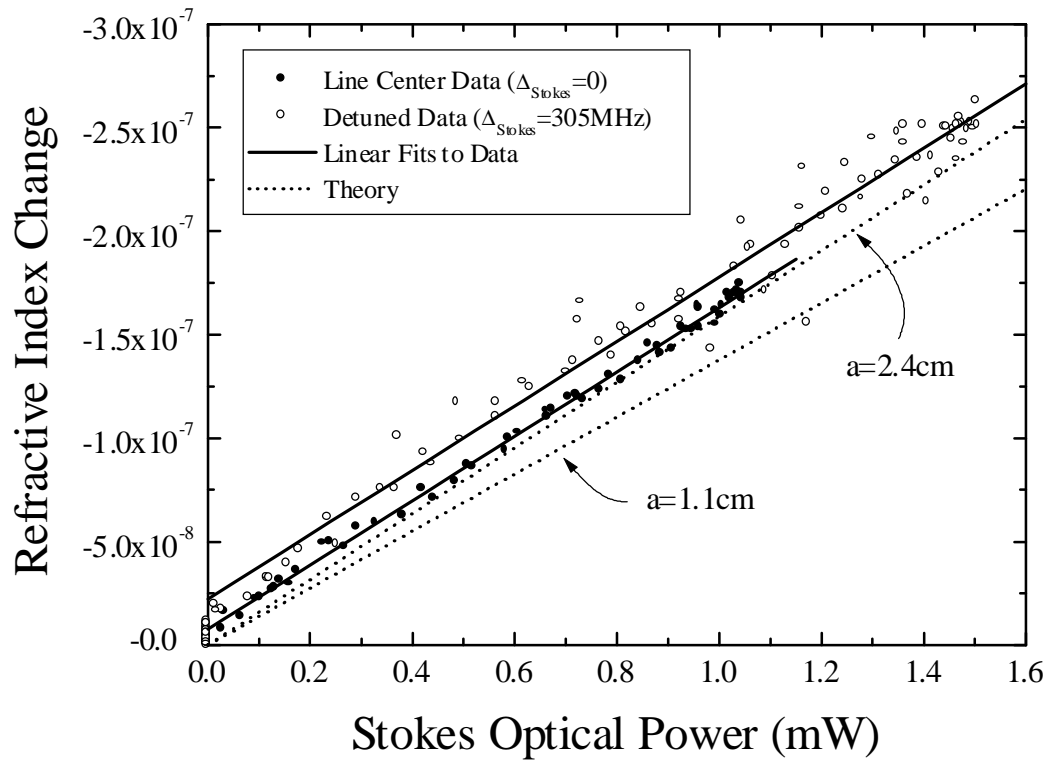


Figure 4

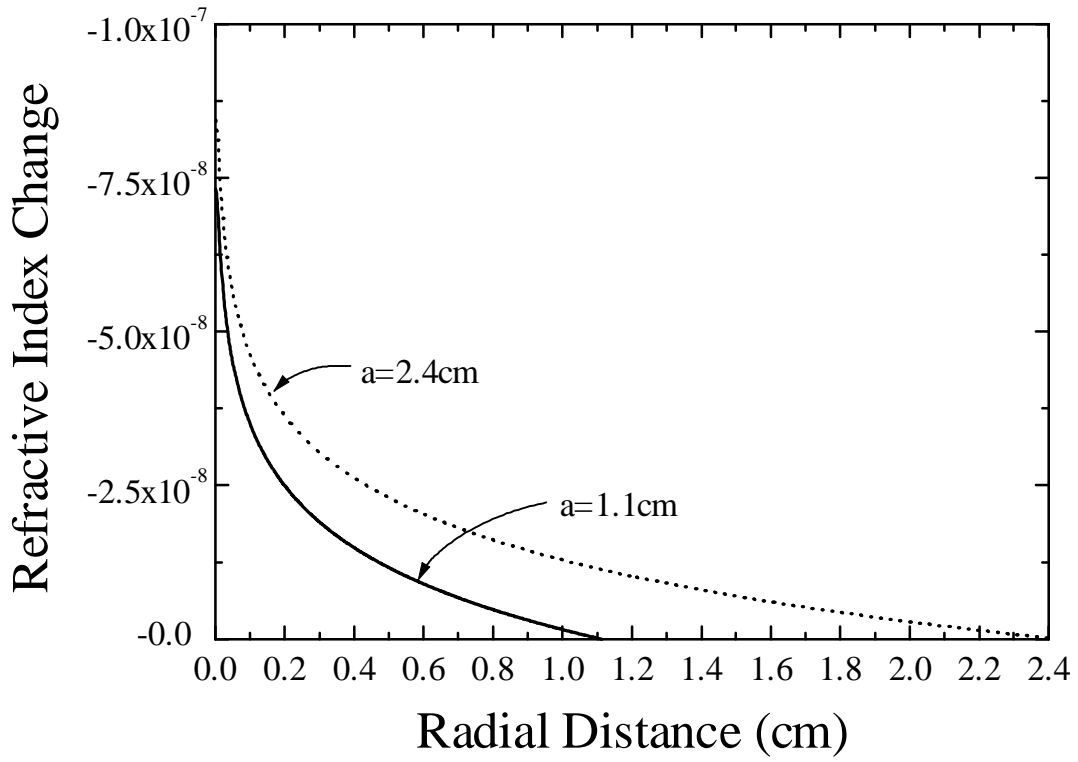


Figure 5

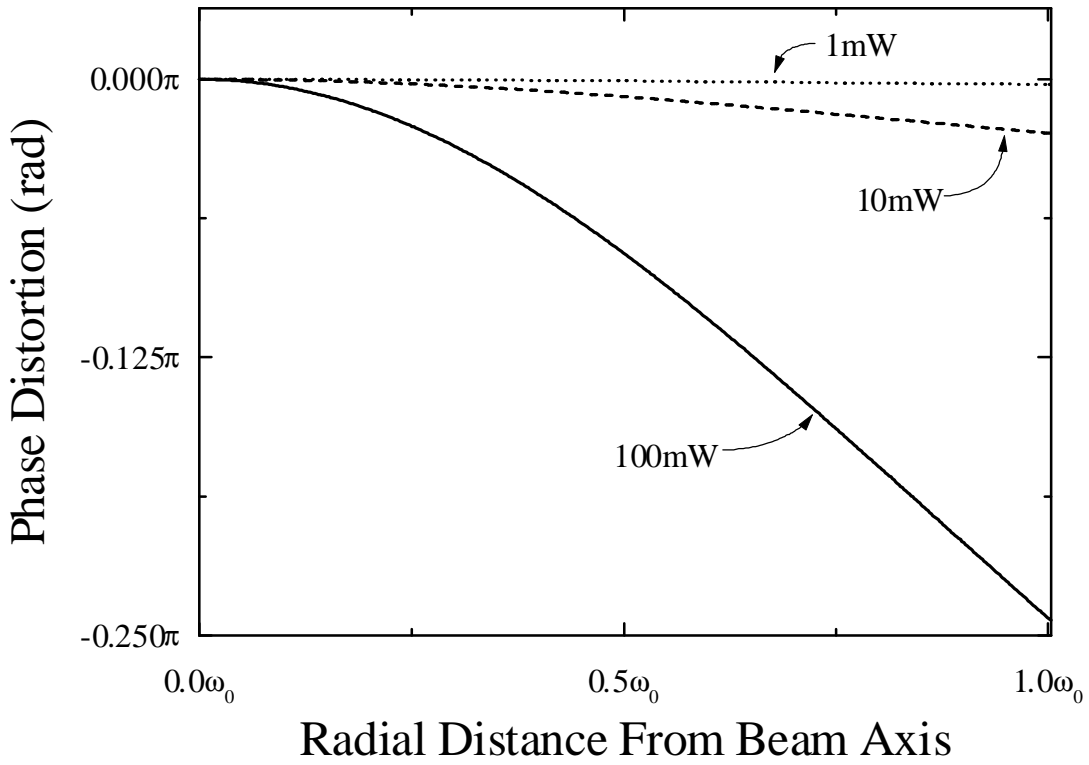


Figure 6

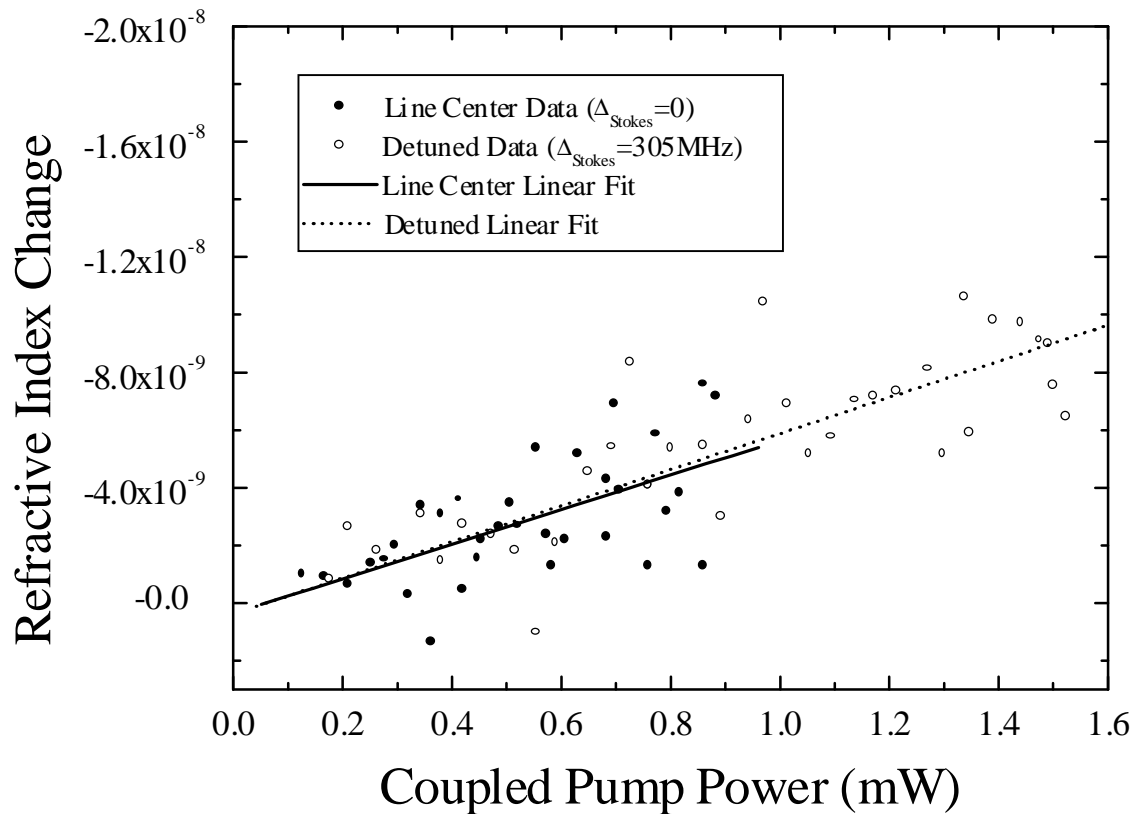


Figure 7